Supplementary Information (SI) for Nanoscale.

Electronic Supplementary Information

Composition controlled synthesis of Pt-Pd-Cu ternary Metal nanoparticles for enhanced electrocatalytic hydrogen evolution reaction

Yu Zhang, Hui Li, Xintong Yan, Wenbo Zhao, Yonghui Ye, Amna Abrar, Qianqian Ren, and Shi Hu*

Department of Chemistry, School of Science, Tianjin Key Laboratory of Molecular Optoelectronic Science, Tianjin University, Tianjin, 300072, China

*Email address: rychushi@gmail.com

Supplemental Experimental Procedures

Chemicals and Materials

Platinum (II) acetylacetonate (96%, $Pt(acac)_2$), iron (III) acetylacetonate (96%, $Fe(acac)_3$), and ruthenium (III) acetylacetonate (97%, $Ru(acac)_3$) were purchased from Tianjin Herwns Technology Co., Ltd., palladium (II) acetylacetonate (99%, $Pd(acac)_2$) was purchased from Shanghai YuanYe Biotechnology Co., Ltd., copper (II) acetylacetonate (>98%, $Cu(acac)_2$) was purchased from Shanghai Titan Technology Co., Ltd., oleylamine (C_{18}:80~90%, OAm), octadecene(>90%, ODE), isopropyl alcohol (99.8%), manganese (II) acetylacetonate (97%, $Mn(acac)_2$), gallium (III) acetylacetonate (99.9%, $Ga(acac)_3$), indium (III) acetylacetonate (99%, $In(acac)_3$), cadmium (II) acetate tetrahydrate (99.5%, $Cd(C_2H_3O_2)_2 \cdot 4H_2O$), tannic acid (Ar, Mw = 1701.20) and hexadecyl-trimethylammonium bromide (90%, CTAB) were purchased from Aladdin Reagent (Shanghai) Co., Ltd., zinc (II) acetylacetonate (97%, $Zn(acac)_2$), Cobalt (III) acetylacetonate (97%, $Co(acac)_3$), nickel (II) acetylacetonate (99%, $Ni(acac)_2$), and rhodium (III) acetylacetonate (99%, $Rh(acac)_3$) were purchased from Shanghai Macklin Biochemical Co., Ltd., ascorbic acid (>99.7%, AA) was purchased from Tianjin Kermio Chemical Reagent Co., Ltd., ethanol (95%), silver (I) nitrate (99.8%, $AgNO_3$), N,N-dimethylformamide (Ar, DMF) and cyclohexane (Ar) were purchased from Tianjin Jiangtian Chemical Technology Co., Ltd., iridium (III) acetylacetonate (98%, $Ir(acac)_3$) was purchased from Shanghai Chempartner Co., Ltd., Tin(II) chloride dihydrate (Ar, $SnCl_2 \cdot 2H_2O$) was purchased from China National Pharmaceutical Group Chemical Reagent Co., Ltd., tetrachloroauric (IV) Acid Tetrahydrate (>99.9%, $HAuCl_4 \cdot 4H_2O$) was purchased from Changzhou Yiding Metal Materials Co., Ltd., bismuth (III) acetate (>99.9%, $Bi(act)_2$)was purchased from Merck Group Germany, nafion was purchased from Dupont, potassium hydroxide (95%, KOH), and lead (II) acetylacetonate (99%, $Pb(acac)_2$) were purchased from Shanghai Meryer Chemical Technology Co., Ltd., and Argon (99.999%) was purchased from Air Liquid Co., Ltd. Glucose (Ar) was purchased from Yuanli Chemical Group Co., LTD. Toluene (Ar) was purchased from Tianjin Bohai Chemical Reagent Co., Ltd. All chemical were used as received without further purification.

Experimental Section

Extended investigation of the reverse reduction of Pt^{2+}

The experimental process mirrored that employed for the synthesis of $PtPd_{0.5}Cu_{0.5}$, with the reaction duration fixed at 1 h. In these trials, OAm or AA were systematically replaced by a blank control, glucose, tannic acid, DMF and toluene, respectively. This substitution strategy enabled a detailed investigation of the individual contributions of OAm and AA to the reaction mechanism.

Extended synthesis of the $PtCu_{0.5}M_{0.5}$ ternary system

The preparation of the ternary metal compounds $PtCu_{0.5}M_{0.5}$ was carried out using the method introduced above, where M is the third element, selected from some metal elements of the third to fifth periods: Mn, Fe, Co, Ni, Zn, Ga, Ru, Rh, Ag, Cd, In, Ir, Au, Pb, Bi. Acetylacetonate salts, due to their high solubility in organic solvents and excellent coordination ability, are selected as metal precursors for synthesis.

Synthesis of $PtCu_{0.5}$-based high entropy alloy NPs

The method used for the preparation of $PtCu_{0.5}$-based high entropy alloy NPs is consistent with the previous one. For the synthesis of $PtCu_{0.5}Pd_{0.5}Sn_{0.5}Pb_{0.5}$, the precursor was replaced with 39.3 mg $Pt(acac)_2$, 13.1 mg $Cu(acac)_2$, 15.2 mg $Pd(acac)_2$, 11.3 mg $SnCl_2 \cdot 2H_2O$, and 20.3 mg $Pb(acac)_2$. Similarly, replace the precursor with 39.3 mg $Pt(acac)_2$, 6.6 mg $Cu(acac)_2$, 7.6 mg $Pd(acac)_2$, 5.7 mg $SnCl_2 \cdot 2H_2O$, and 10.2 mg $Pb(acac)_2$ for the synthesis of $PtCu_{0.25}Pd_{0.25}Sn_{0.25}Pb_{0.25}$ NPs.

The synthesis process for the metal-supported samples

Four times the amount of Vulcan XC-72 carbon black was measured based on the theoretical metal mass of different components, and put into a 50 mL round-bottom flask. Then, add 20 mL of ethanol and stir magnetically for 2 h to fully disperse the carbon black in ethanol. Disperse the product in cyclohexane from the previous step into the carbon black solution at a rate of 1 mL/min, and continue stirring for 12 h. Subsequently, wash the carbon-loaded sample three times by centrifugation with ethanol. Place the centrifuged product in a cool, ventilated area to dry for subsequent characterization tests.

Characterization

Characterization of as-synthesis NPs

The morphology and HRTEM of the NPs were probed on JEOL-1230 with an accelerating voltage of 100 kV and JEM-ARM 200F field emission transmission, operating at 200 kV. EDS-Mapping images were captured with JED-2200, employing a pixel dwell time of 5 ms for a 512 * 512-pixel frame. XRD pattern of the samples was obtained via Bruker D8-focus diffractometer using a Cu Kα source ($\lambda_{\mathrm{Cu\ K\alpha}}$ = 1.5406Å) with a testing voltage of 40 kV and current of 40 mA. The scan rate was set at a rate of 8 °/min, ranging from 20° to 80°. XPS measurement was carried out using an Al K_{α} source, with the chamber pressure below 4×10^{-9} Torr. Calibration for C_{1s} was adjusted to 284.78 eV to mitigate the impact of the charge accumulation.

The measurement of electrochemical active surface area

Place the activated sample in CO-saturated 1 M KOH and conduct the potentiostatic experiment (it) at a potential of 0.08 V vs. RHE for 600 s. Subsequently, transfer the CO-adsorbed sample to Ar-saturated 1 M KOH and perform a CV scan from 0.05 to 1.1 V vs. RHE at a scan rate of 10 mV/s. This will be used for subsequent electrochemically active surface area calculation. H_{UPD} is also an effective method for calculating the electrochemical active surface area. It utilizes metals with H-specific adsorption properties, such as Pt or Pd, to form monolayer adsorption at the reduction potential of H. The electrode window ranges from 0.05 V to 0.5 V vs. RHE. The electrochemical active surface area can be calculated based on the peak area of H_{UPD} from the CV curve[26]. The relative calculating equations are listed below.

$$ECSA = Q/qvm\ (CO\ Stripping)\ \#(1)$$

$$ECSA = Q_H/420\mu C{\cdot}cm^{-2}\ (H_{UPD})\ \#(2)$$

The stability test of sample

To simulate an accelerated durability test, the samples were cycled 5000 times within a potential window ranging from 0.05 V to 1.1 V vs. RHE. Subsequently, LSV experiment was conducted to assess the performance of the samples after the stability test.

Results and discussion

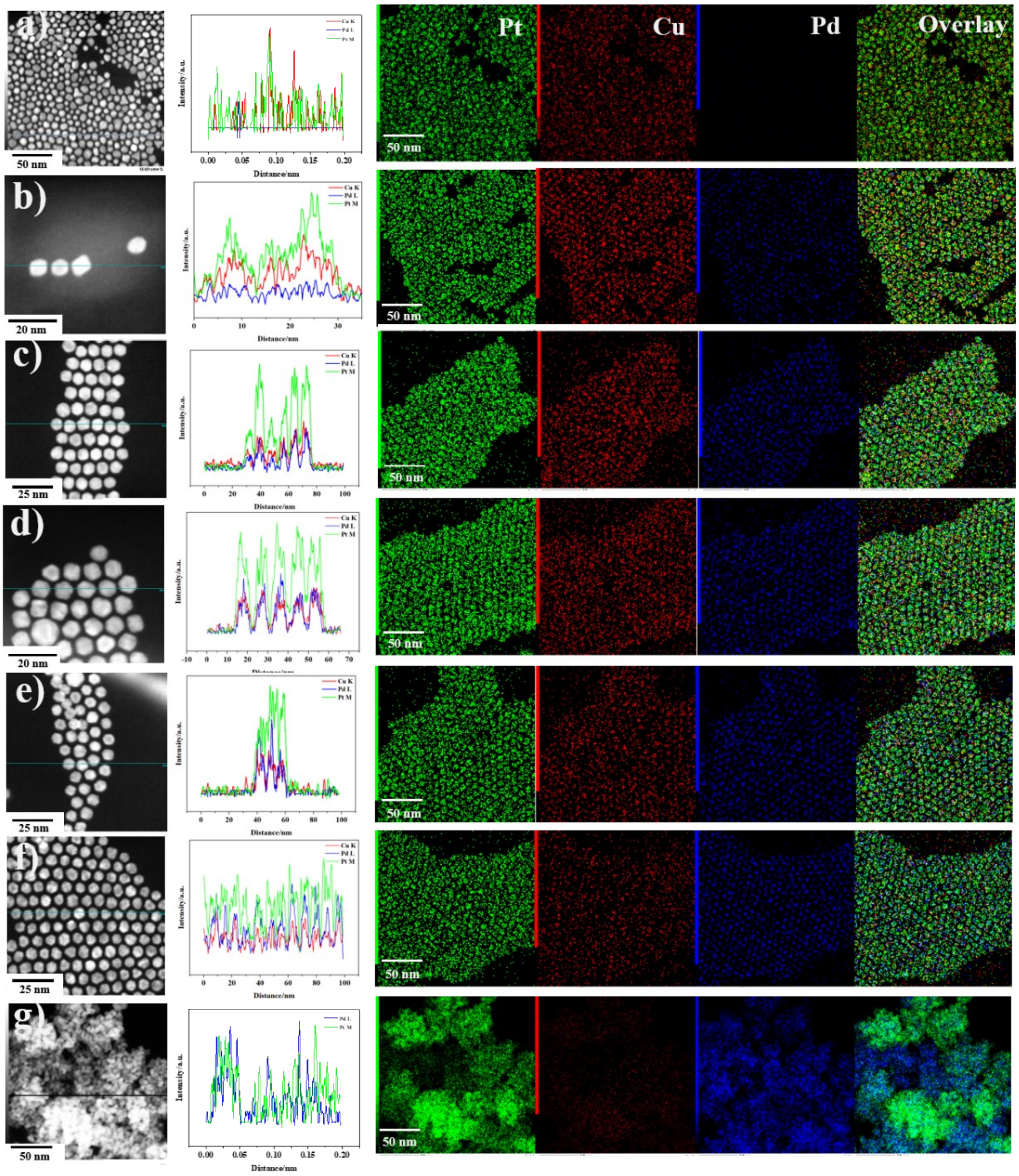

Figure S1. Element distribution mapping and line scan results for different Pd/Cu feed ratios a) PtCu, b) $PtPd_{0.2}Cu_{0.8}$, c) $PtPd_{0.4}Cu_{0.6}$, d) $PtPd_{0.5}Cu_{0.5}$, e) $PtPd_{0.6}Cu_{0.4}$, f) $PtPd_{0.8}Cu_{0.2}$, and g) PtPd, where red represents Cu, blue represents Pd, and green represents Pt.

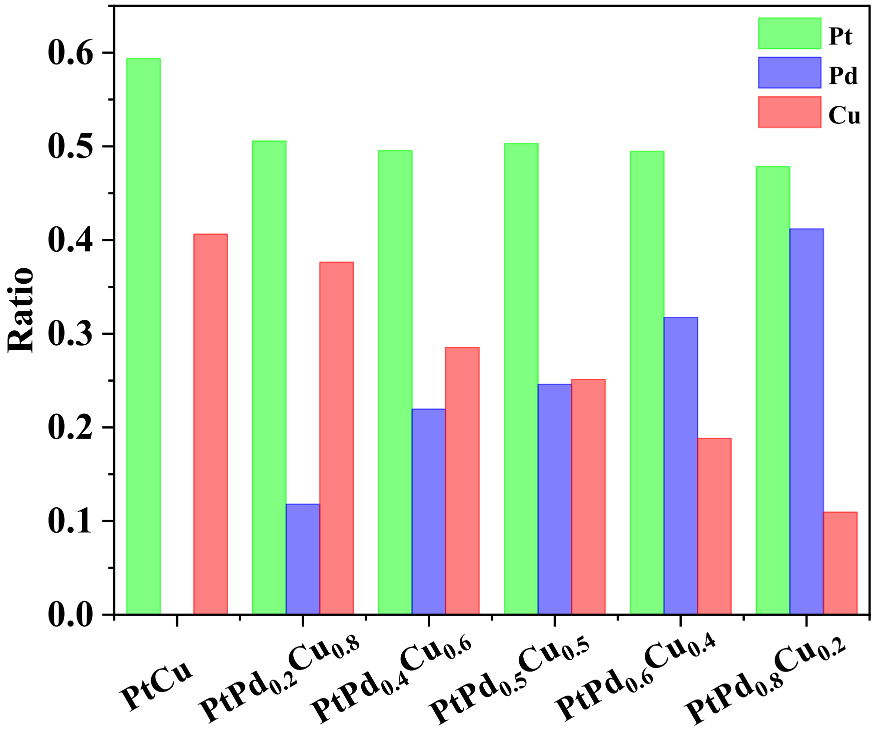

Figure S2. EDS quantitative analysis results of PtCu, $PtPd_{0.2}Cu_{0.8}$, $PtPd_{0.4}Cu_{0.6}$, $PtPd_{0.5}Cu_{0.5}$, $PtPd_{0.6}Cu_{0.4}$, and $PtPd_{0.8}Cu_{0.2}$ samples.

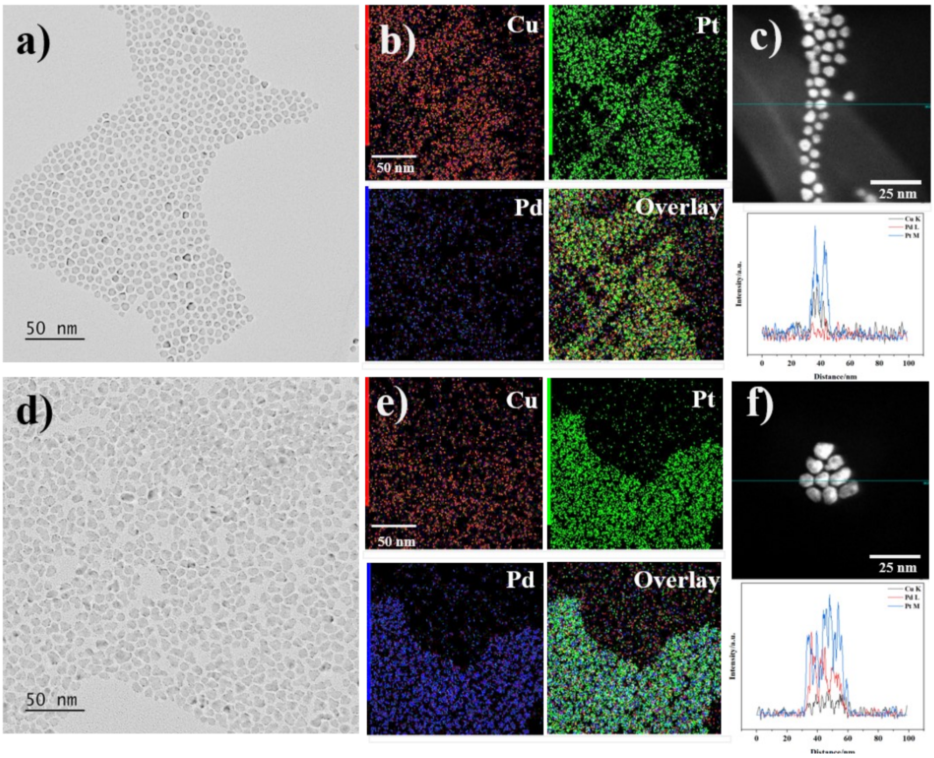

Figure S3. Characterization of morphology and elemental distribution of the a-c) $PtPd_{0.05}Cu_{0.95}$ sample and d-f) $PtPd_{0.05}Cu_{0.95}$ sample. a) and d) TEM image, b) and e) EDS elemental distribution mapping, c) and f) line scanning image with the elemental distribution

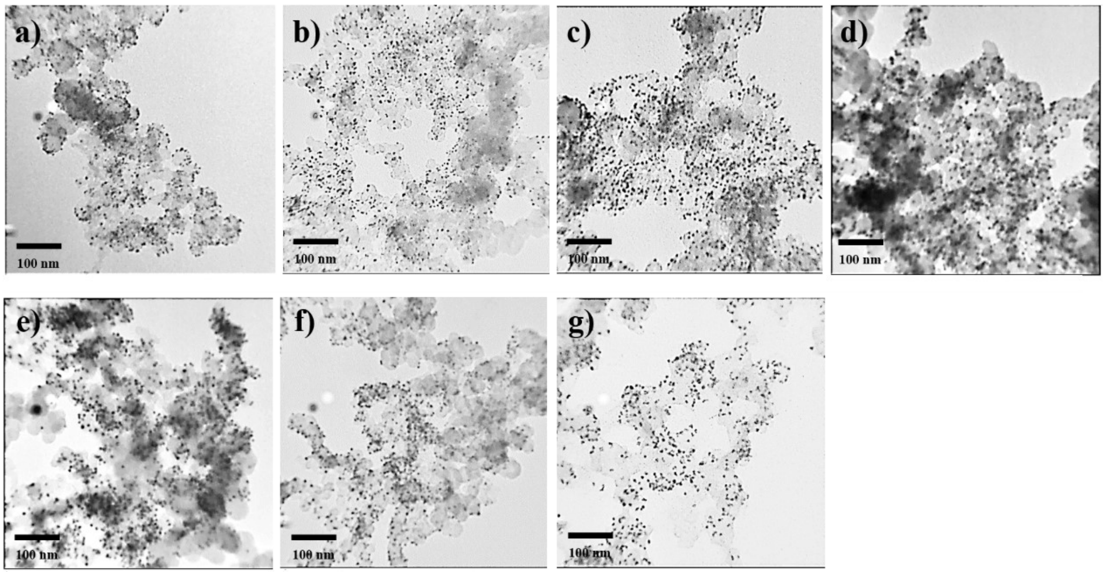

Figure S4. Low-magnification transmission electron microscopy images of $PtPd_xCu_{1-x}$ samples supported on Vulcan XC-72 carbon black a) $PtPd_{0.05}Cu_{0.95}$, b) $PtPd_{0.2}Cu_{0.8}$, c) $PtPd_{0.4}Cu_{0.6}$, d) $PtPd_{0.5}Cu_{0.5}$, e) $PtPd_{0.6}Cu_{0.4}$, f) $PtPd_{0.8}Cu_{0.2}$, and g) $PtPd_{0.95}Cu_{0.05}$.

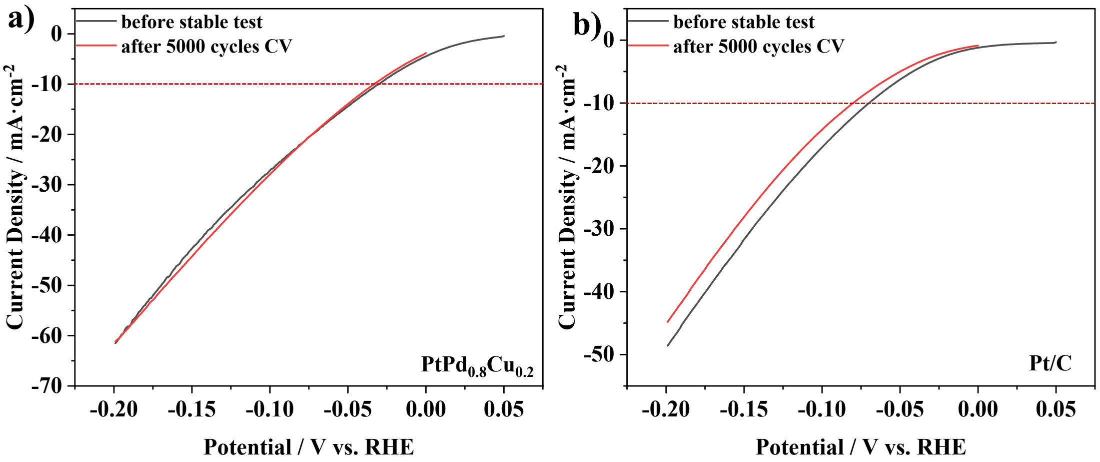

Figure S5. Stability test results for a) the $PtPd_{0.8}Cu_{0.2}$ sample and b) the commercial Pt/C sample: Comparative analysis of the electrocatalysts before and after undergoing a 5000 CV test.

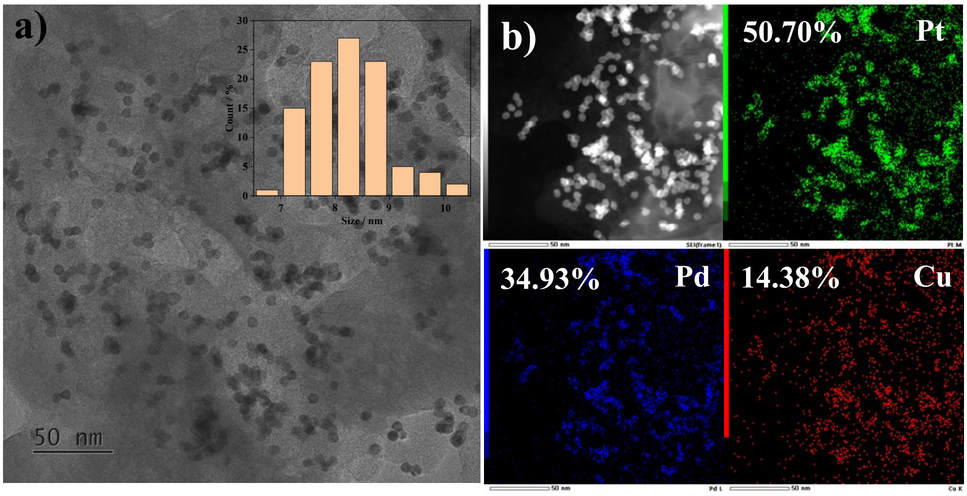

Figure S6. a) TEM characterization, b) EDS mapping test pf $PtPd_{0.8}Cu_{0.2}$ after 5000 cycles CV test.

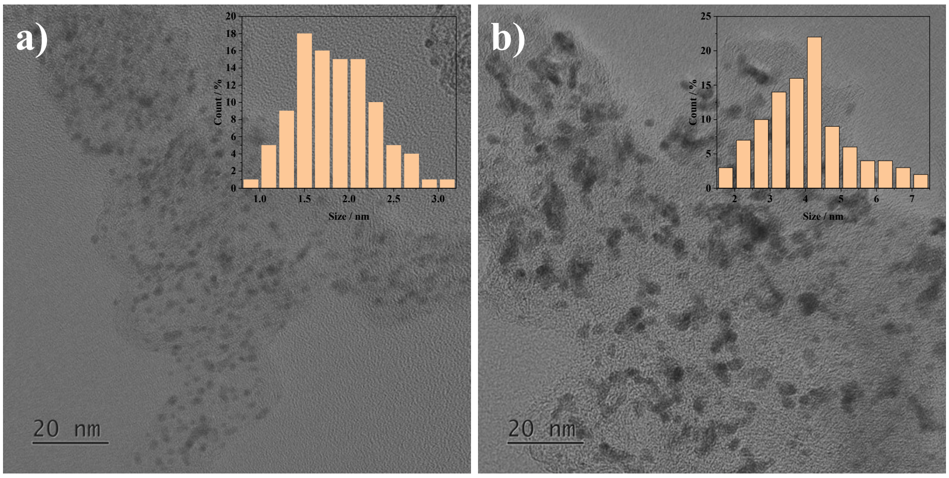

Figure S7. a) TEM characterization of commercial Pt/C before and after 5000 cycles CV test.

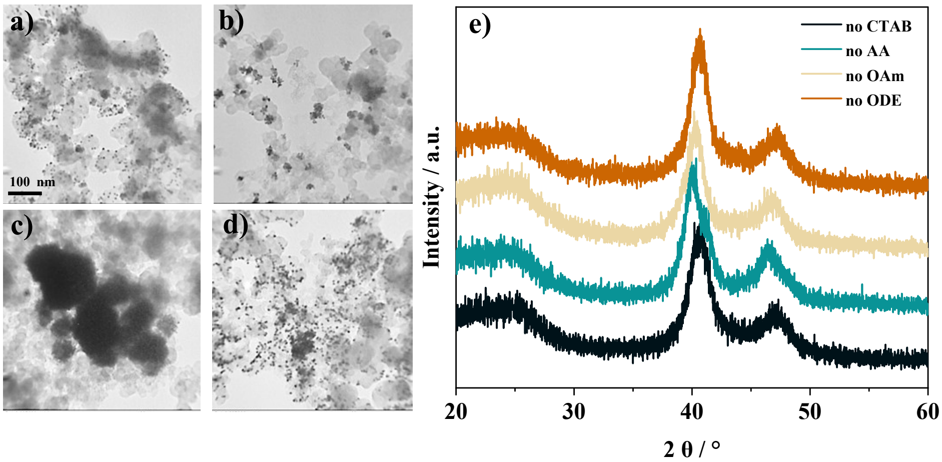

Figure S8. Investigation the synthesis factors for $PtPd_{0.5}Cu_{0.5}$ a) without CTAB addition, b) without AA addition, c) without OAm addition, d) without ODE addition, e) XRD patterns of the samples mentioned above.

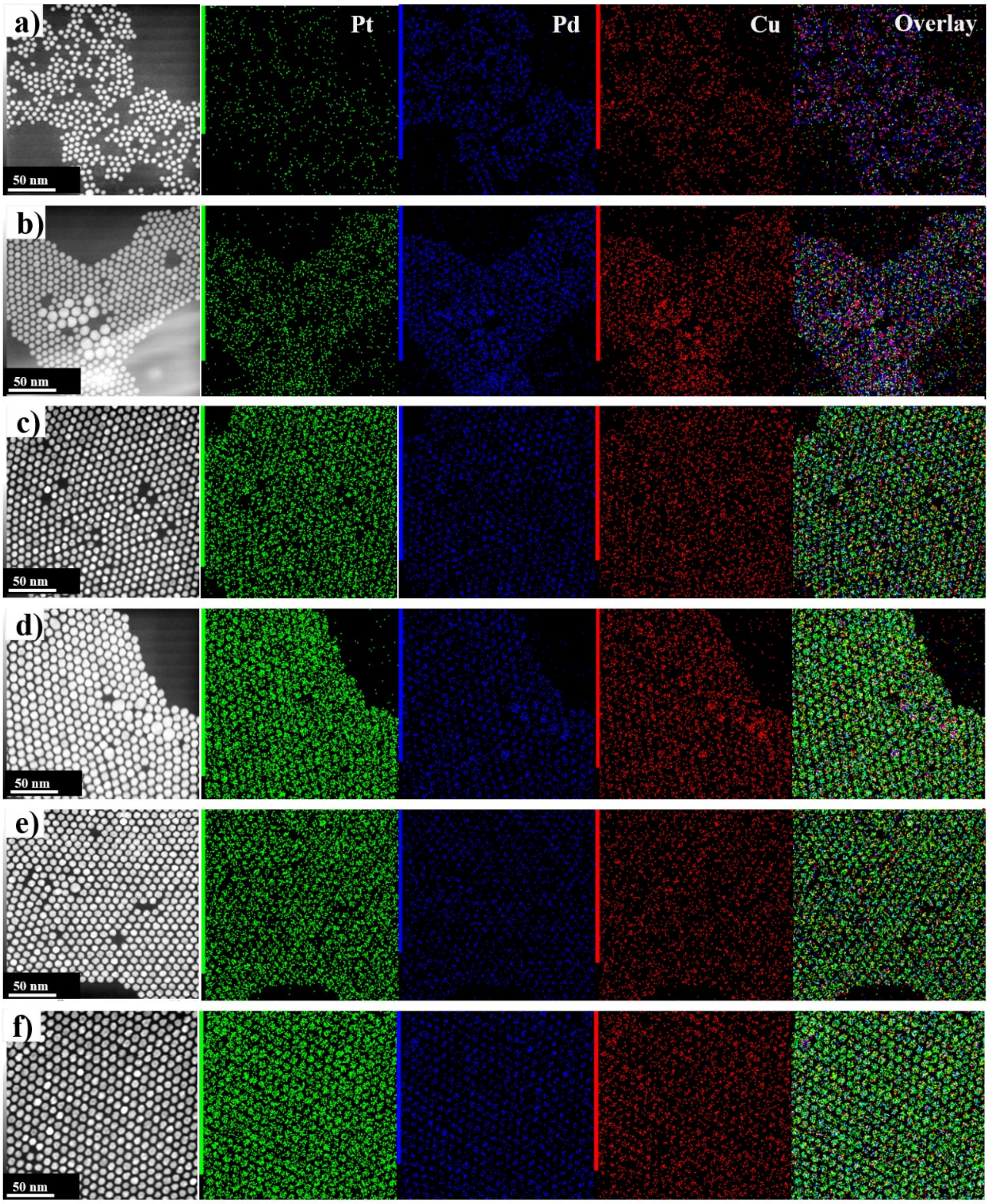

Figure S9. Investigation of the effect of synthesis time on the products of $PtPd_{0.5}Cu_{0.5}$. The HADDF-STEM images long with the element distribution mapping for reaction times a) 0.5 h, b) 1 h, c) 2 h, d) 3 h, e) 6 h, and f) 9 h are shown, here, red represents Cu, blue represents Pd, and green represents Pt.

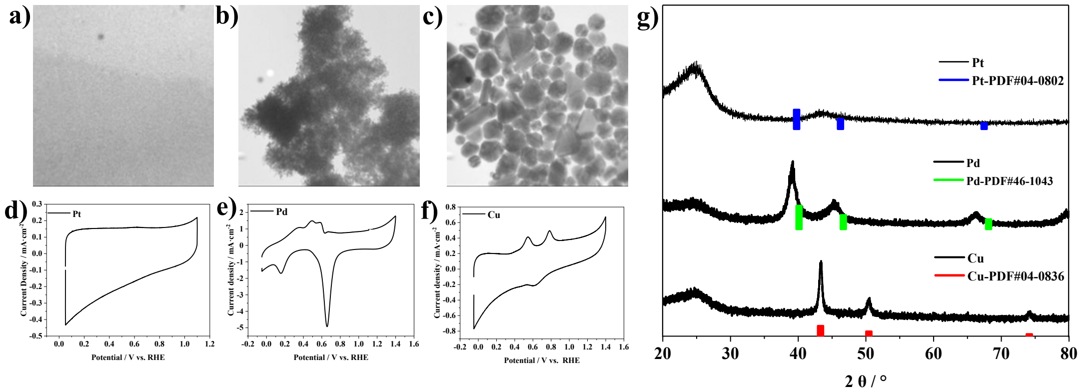

Figure S10. Morphology at low magnification for a) Pd, b) Cu, c) Pt, electrochemical CV test results in 1 M KOH for d) Pt, e) Pd, f) Cu, g) XRD diffraction patterns of synthesized Pt, Pd, and Cu samples.

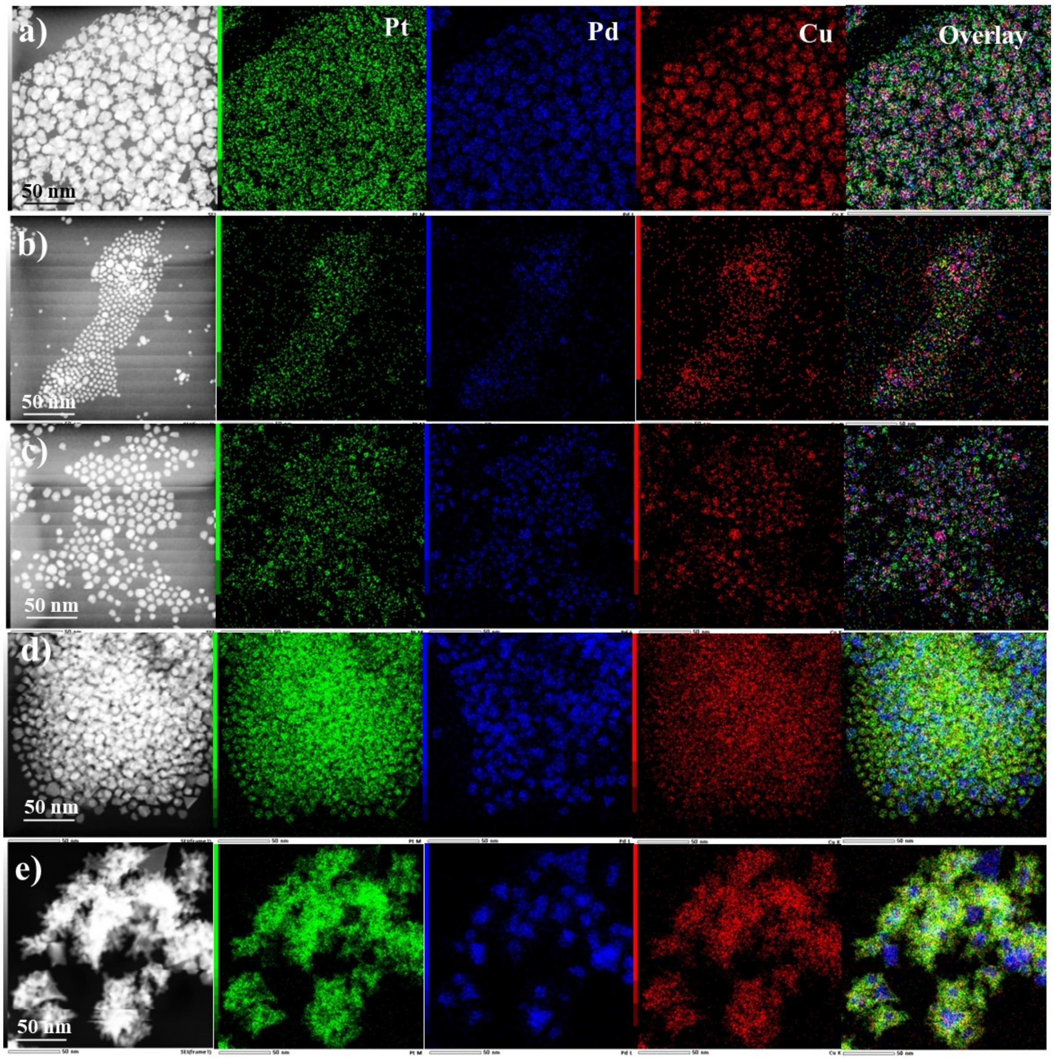

Figure S11. EDS mapping characterization of $PtPd_{0.5}Cu_{0.5}$ reacted at 180 °C for 1 h with AA substituted with a) blank, b) glucose, c) tannic acid; with OAm substituted with d) N, N-dimethylamide, e) toluene.

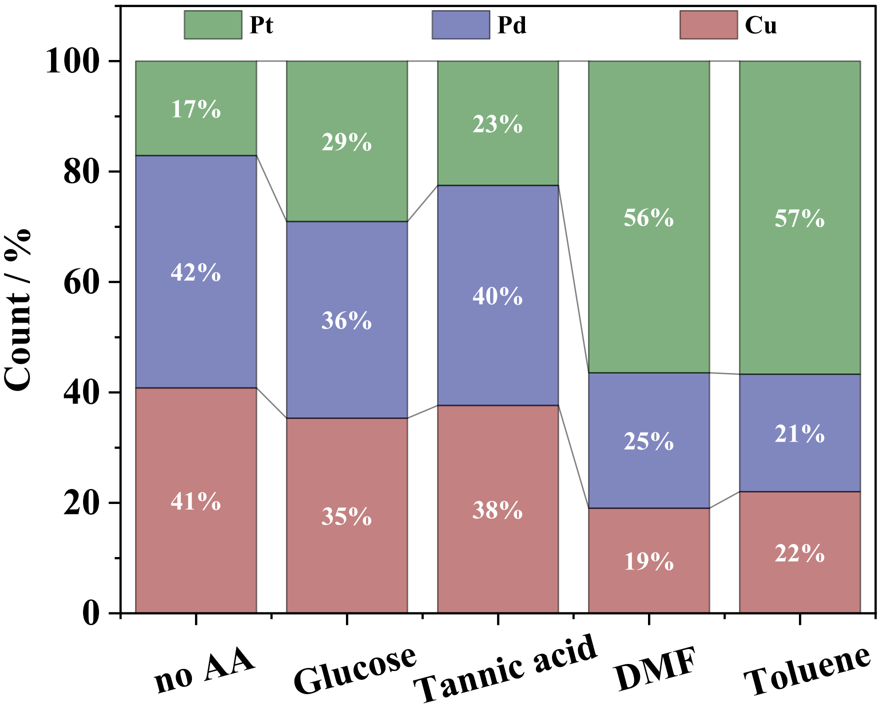

Figure S12. The atomic element ratio of the related samples characterized by EDS mapping.

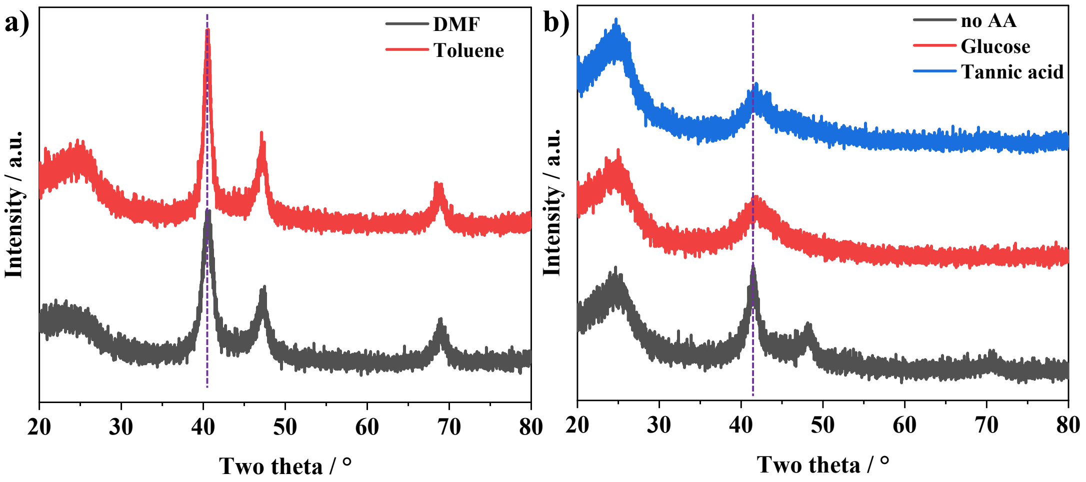

Figure S13. The XRD pattern of the related samples in the investigation of the factors influencing the reverse reduction of Pt^{2+}.

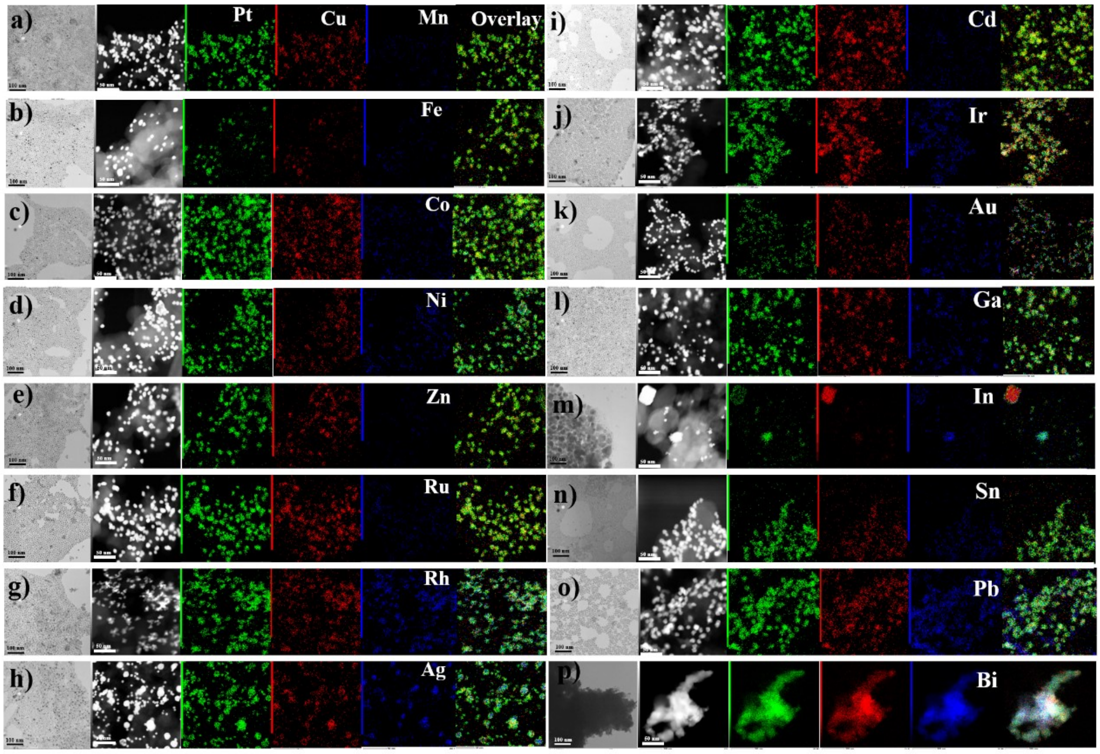

Figure S14. TEM images under low magnification, HADDF-STEM and EDS mapping images under high magnification, where red represents Cu, green represents Pt, and blue represents M elements a) $PtCu_{0.5}Mn_{0.5}$, b) $PtCu_{0.5}Fe_{0.5}$, c) $PtCu_{0.5}Co_{0.5}$, d) $PtCu_{0.5}Ni_{0.5}$, e) $PtCu_{0.5}Zn_{0.5}$, f) $PtCu_{0.5}Ru_{0.5}$, g) $PtCu_{0.5}Rh_{0.5}$, h) $PtCu_{0.5}Ag_{0.5}$, i) $PtCu_{0.5}Cd_{0.5}$, j) $PtCu_{0.5}Ir_{0.5}$, k) $PtCu_{0.5}Au_{0.5}$, l) $PtCu_{0.5}Ga_{0.5}$, m) $PtCu_{0.5}In_{0.5}$, n) $PtCu_{0.5}Sn_{0.5}$, o) $PtCu_{0.5}Pb_{0.5}$, and p) $PtCu_{0.5}Bi_{0.5}$.

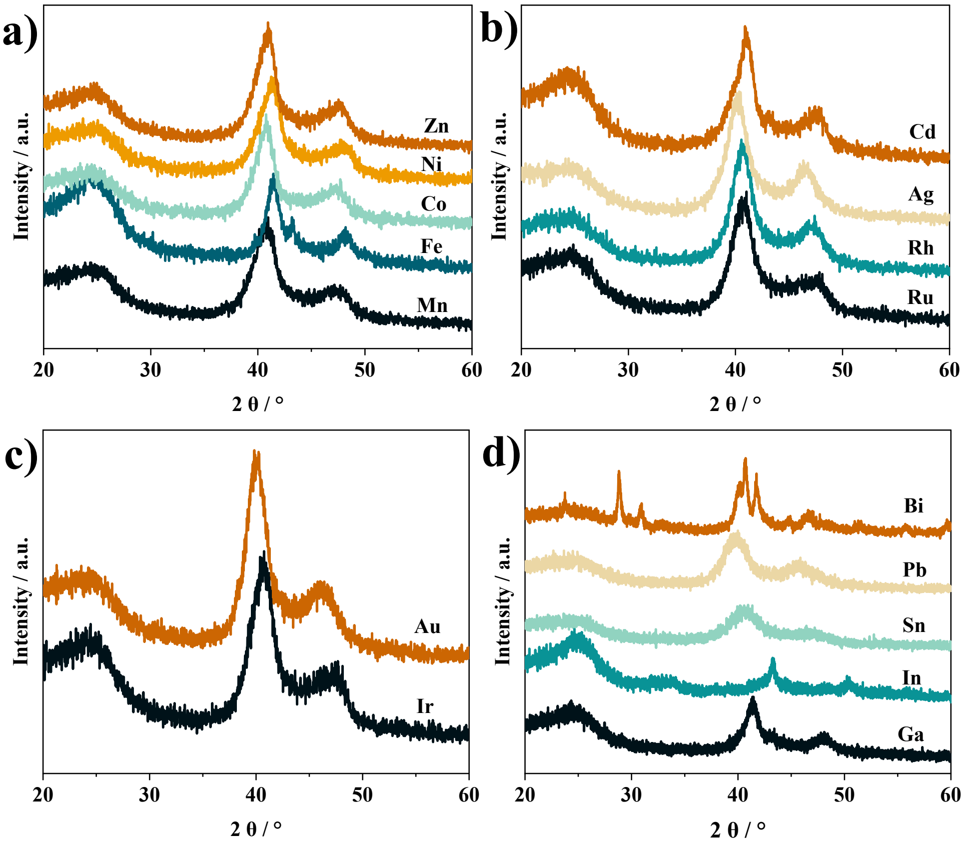

Figure S15. XRD diffraction patterns of PtCu$_{0.5}$M$_{0.5}$ samples a) M is one of Mn, Fe, Co, Ni, Zn, b) M is one of Ru, Rh, Ag, Cd, c) M is one of Ir, Au, and d) M is one of Ga, In, Sn, Pb, Bi.

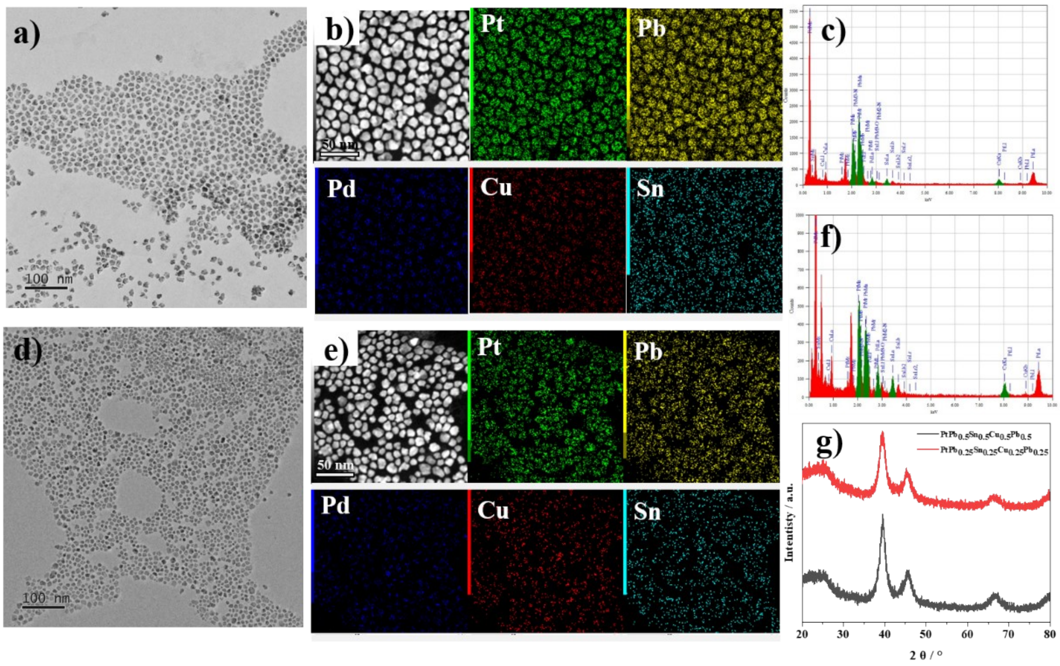

Figure S16. Characterization of PtCu$_{0.5}$Sn$_{0.5}$Pb$_{0.5}$Pd$_{0.5}$ and PtCu$_{0.25}$Sn$_{0.25}$Pb$_{0.25}$Pd$_{0.25}$. a) and d) TEM image, b) and e) EDS mapping image, c) and f) EDS quantitative analysis results, g) XRD spectrum, and h) ICP-OES test results.

Table S1. EDS quantitative analysis results of $PtCu_{0.5}M_{0.5}$ samples

Samples	Pt	Cu	M
$PtCu_{0.5}Mn_{0.5}$	66.32%	31.05%	2.63%
$PtCu_{0.5}Fe_{0.5}$	44.22%	45.27%	10.51%
$PtCu_{0.5}Co_{0.5}$	65.04%	30.76%	4.20%
$PtCu_{0.5}Ni_{0.5}$	60.46%	25.46%	14.08%
$PtCu_{0.5}Zn_{0.5}$	66.32%	31.05%	1.48%
$PtCu_{0.5}Ru_{0.5}$	68.67%	30.34%	0.99%
$PtCu_{0.5}Rh_{0.5}$	48.11%	29.89%	22.00%
$PtCu_{0.5}Ag_{0.5}$	52.31%	18.42%	29.27%
$PtCu_{0.5}Cd_{0.5}$	58.14%	41.715	0.15%
$PtCu_{0.5}Ir_{0.5}$	57.08%	37.06%	5.86%
$PtCu_{0.5}Au_{0.5}$	46.86%	31.96%	21.18%
$PtCu_{0.5}Ga_{0.5}$	51.82%	44.80%	3.38%
$PtCu_{0.5}In_{0.5}$	/	/	/
$PtCu_{0.5}Sn_{0.5}$	48.78%	30.69%	20.53%
$PtCu_{0.5}Pb_{0.5}$	53.29%	23.83%	22.88%
$PtCu_{0.5}Bi_{.5}$	/	/	/

Table S2. ICP-OES test result for $PtCu_{0.5}$-based high entropy alloy

Elements	$PtPd_{0.5}Cu_{0.5}Sn_{0.5}Pb_{0.5}$	$PtPd_{0.25}Cu_{0.25}Sn_{0.25}Pb_{0.25}$
Pt	39.75%	52.50%
Pd	15.51%	12.42%
Pb	19.89%	14.20%
Sn	5.60%	8.74%
Cu	19.25%	12.13%